Physical Mechanism for the Tallahassee, Florida, Minimum Temperature Anomaly

A. BIROL KARA, JAMES B. ELSNER, AND PAUL H. RUSCHER

Department of Meteorology, The Florida State University, Tallahassee, Florida

(Manuscript received 12 November 1996, in final form 17 March 1997)

ABSTRACT

Nighttime minimum temperatures at the Tallahassee Regional Airport (TLH) are colder in comparison with surrounding locations and other parts of the city, especially during the cool season (TLH minimum temperature anomaly). These cold events are examined using the one-dimensional Oregon State University atmospheric boundary layer (ABL) model including a two-layer model of soil hydrology. The model is used for 12-h forecasts of the ABL parameters, such as surface fluxes, surface inversion height, and minimum temperature when clear, calm synoptic conditions existed over the region at night. The minimum temperature forecasts are performed at TLH and a nearby location. Cooling in the surface inversion layer is examined in terms of turbulence and clear-air radiative effects, and it is confirmed that the lower temperatures at TLH are related to the clear-air radiative cooling even in the lower part of the inversion layer but not to cold-air drainage. Stability, ABL height, and surface inversion height are examined with respect to a potential temperature curvature. Turbulent exchanges in the surface boundary layer are also taken into account. The model is able to simulate the nocturnal evolution of air temperatures well. Besides the soil moisture, the value of the roughness length momentum has a substantial effect on temperature forecasts in the model. The best overall agreement for the minimum temperature prediction over TLH is obtained using equal values for the roughness lengths of heat and momentum. Finally, use of the ABL model with its surface energy balance and crude radiative parameterization package under negligible synoptic-scale forcing can be valuable to a forecaster in predicting the daily maximum temperature drop.

1. Introduction

A rapid diurnal drop in surface air temperature tends to be most pronounced under clear nighttime skies, light winds, and dry air—such conditions favor strong inversions near the ground. This drop in air temperature can be explained in terms of radiative flux divergence (Quinet and Vanderborght 1996). When the temperature gradient is large during the clear night, heating processes in the ground are important to the surface energy balance. Also, vertical exchanges influence the temperature structure at the ground in the presence of turbulence. It is known that the atmospheric boundary layer is stably stratified due to radiative cooling at the land surface during clear nights, and several studies show that cooling rates near the ground can be substantial (Garratt and Brost 1981; Carlson and Stull 1986). On the other hand, when there is a temperature inversion near the surface level, radiative heating from the warmer air aloft is expected (Stull 1983). Several studies have examined the nocturnal atmospheric boundary layer (ABL) in terms of clear-air radiative cooling (e.g., Anfossi et al. 1976; Klöppel et al. 1978). The lower ABL is mostly affected by turbulence, while the upper layer is affected by clear-air radiative cooling at night (André and Mahrt 1982).

The interaction between boundary layer development and soil characteristics due to vegetation is also very important (Pan and Mahrt 1987). Because the structure of the nocturnal ABL plays an important role for the estimation of minimum temperature, surface heat fluxes and boundary layer height are mainly discussed in this investigation. Examination of surface fluxes (sensible and latent) is of crucial importance since they determine the mean profiles of the surface layer and identify the dynamics of the ABL (e.g., Beljaars and Holtslag 1991; Nieuwstadt and Driedonks 1979). Observations and numerical model results show that the surface fluxes are mainly affected by surface properties (e.g., Xinmei and Lyons 1995; Holtslag and Ek 1996). Over land, the surface fluxes are influenced by the interaction of the vegetated surface and the atmosphere. This is especially important for short-range weather forecasting (e.g., Kondo et al. 1992; Beljaars and Holtslag 1991). Determination of ABL height is also important since fluxes, wind shears, clouds, and turbulent intensities in the boundary layer depend on it. Especially for the nighttime stable boundary layer, both the measurement and prediction of the ABL height are more difficult and less reliable. The rate equations for the stable ABL height and inversion height are discussed in many papers and several different approaches have been used to deter-

Corresponding author address: A. Birol Kara, Department of Meteorology, The Florida State University, Tallahassee, FL 32306-4520.
E-mail: birol@met.fsu.edu

© 1998 American Meteorological Society

Unauthenticated | Downloaded 03/27/23 11:23 PM UTC

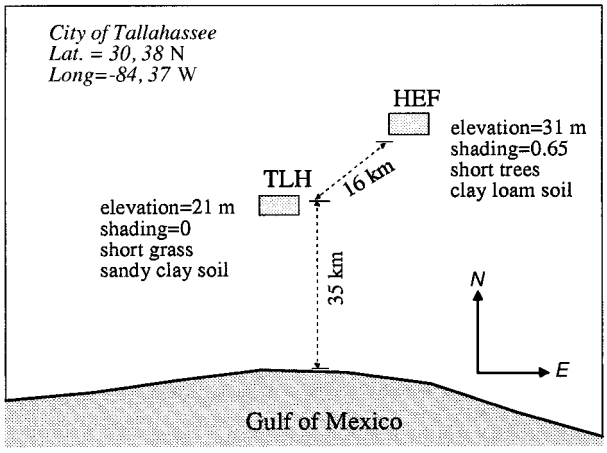

FIG. 1. Two sites (TLH and HEF) used in this study. Several surface characteristics are also indicated at each site.

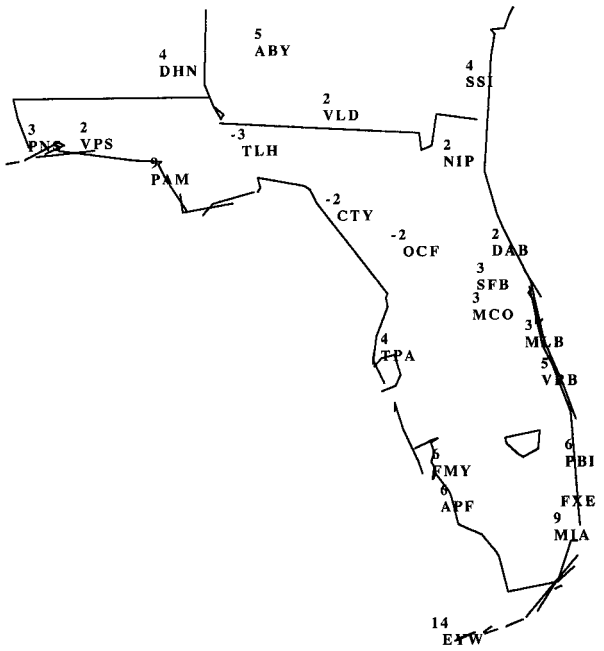

FIG. 2. Observed minimum temperatures (°C) in the extreme southeastern United States on 7 February 1995. The locations surrounding TLH are Dothan (DHN), Albany (ABY), Valdosta (VLD), Panama City (PAM), Valparaiso (VPS), and Jacksonville (NIP).

mine these parameters (e.g., Nieuwstadt 1980; Yamada 1979; Yu 1978). In this paper, we follow the definition of André and Mahrt (1982) for the determination of surface inversion height since it involves a thicker layer close to the surface. The ABL depth is expressed in terms of a bulk Richardson number including the influence of thermals. Radiative fluxes and atmospheric stability within the ABL are necessary for accurate prediction of the potential evaporation. With the existence of dry soil, the evaporation rate is controlled by the soil moisture gradient in the upper part of the soil (Pan and Mahrt 1987). Since ABL parameters are of crucial importance, the temperature drop at night is investigated with respect to these parameters.

The regional airport, located on the southwest side of the city of Tallahassee, Florida, experiences a pronounced minimum temperature bias toward colder readings compared with nearby locations in the community. This TLH minimum temperature anomaly is most frequent during the cooler, drier months and may occur at other locations in northern Florida. It has been suggested that the reason for this minimum temperature anomaly has more to do with radiation than with cold-air drainage (Elsner et al. 1996). In this study, we mainly focus on the reasons for this minimum temperature anomaly by evaluating ABL model forecasts made for TLH and for a nearby location in the city. We confirm that the cold-air drainage hypothesis previously used to explain the cold temperatures at TLH is not valid, and instead the phenomenon may be due entirely to radiative processes. The analysis begins with a description of the chosen sites and the various data collected for the study. This is followed by a discussion of the boundary layer parameterizations including the model initialization. Model forecasts are analyzed in section 4, results and discussions are given in section 5, and conclusions are provided in section 6.

2. Description of sites and data

The Tallahassee Regional Airport (TLH) is in the central panhandle of northern Florida. It has an elevation of 21 m above sea level and is approximately 35 km from the Gulf of Mexico coast, as shown in Fig. 1. The city lies near the coastal plain (see also Fig. 2) but far from the modifying influences of the ocean on clear, calm nights.

TLH often has the lowest minimum temperature in the southeastern United States (especially Alabama and Georgia) 1–4 days after passage of a cold front in spite of its more southerly location and its proximity to the Gulf of Mexico. Figure 2 shows the minimum temperatures observed on 7 February 1995, indicating the coldest minimum temperature at TLH compared with nearby locations [note that Cross City (CTY) and Ocala (OCF) may also be experiencing a similar condition on this particular occasion]. Figure 3 shows temperature changes, cloudiness, mean sea level pressure, and wind speed and direction for a 12-h period at night when clear, calm synoptic conditions existed at TLH on 7 February 1995. The minimum temperature is observed at around 0600 UTC just prior to the arrival of a scattered cloud layer. There is no significant change in the pressure tendency during the night. The turbulence is a minor contributor during the calm, fair nights at TLH since the lower atmosphere is very stable, as will be discussed later. It has been suggested (see also Fig. 1) that the TLH minimum temperature anomaly is very local and

Unauthenticated | Downloaded 03/27/23 11:23 PM UTC

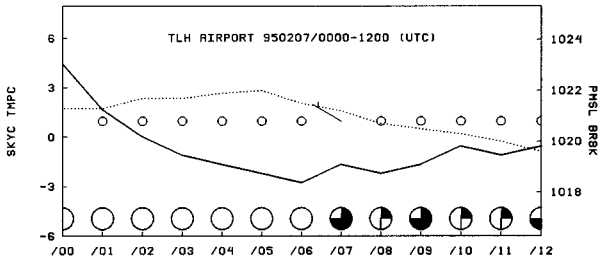

FIG. 3. Observed minimum temperature (TMPC, °C, solid line), mean sea level pressurre (PMSL, hPa, dotted line), cloud cover (SKYC, large circles), and wind speed and direction (BRBK, kt) at TLH for the calm, clear night on 7 February 1995. Small open circles represent calm wind speed.

does not represent the conditions over most of the city of Tallahassee.

Here, we use 0000 UTC upper-air soundings at TLH combined with surface observations from an unofficial site located approximately 16 km northeast of TLH in an urban forest at an elevation of approximately 31 m (see also Fig. 1). The site has been maintained by Professor H. E. Fuelberg and will hereafter be referred to as HEF. The HEF site is a liquid-in-glass minimum thermometer housed in a standard wooden shelter. To emphasize the local nature of the TLH minimum temperature anomaly, we note that the number of freezes ($T \leq 0$°C) at TLH over the past 8 years (1988–95) is nearly double the number at HEF (236:130). We assume that upper-air characteristics are the same for both locations since they are in close proximity. The surface observations (mean sea level pressure, wind speed, direction, temperature, dewpoint temperature) were taken every day during 1990–95 at TLH and HEF. We determined 67 days where the wind was calm and cloud cover was less than 30% at night during this period. Figure 3 is a typical example from the days selected. During the selection of clear nights, no effort was made to look at the large-scale flow to determine if advection would be an important factor as it was felt that the criterion of light winds would preclude this possibility. We examined 14 out of 67 cases to determine soil moisture and extracted these cases from the rest of the analysis, as will be explained later. As a result, when considering the 53 remaining cases, Fig. 4a shows that the minimum temperatures observed at TLH are approximately 1°–4°C lower than the ones measured at HEF during calm, clear nights. The surface mixing ratio values (g kg^{-1}) calculated from the dewpoint temperatures for the same period exhibit a relatively small ratio between TLH and HEF (Fig. 4b). Large mixing ratio values at HEF also verify the higher dewpoint temperatures at this location. Even though the minimum temperatures at TLH are always colder than the ones measured at HEF under these special conditions, there are some cases where the mixing ratio values are larger at HEF than at TLH due, in part, to slightly higher surface pressures and the presence of vegetation. The average surface pressure at HEF is 1020.8 hPa, while at TLH it is 1021.4 hPa when considering all 53 days at around 0700 LST (local standard time).

3. Boundary layer parameterizations

The ABL model is described with eddy diffusivity (K theory) and countergradient transport terms (Troen and Mahrt 1986). The ABL model is coupled with an active two-layer soil model (Mahrt and Pan 1984) and a primitive plant canopy model (Pan and Mahrt 1987). In the following section, we summarize the equations used in the models.

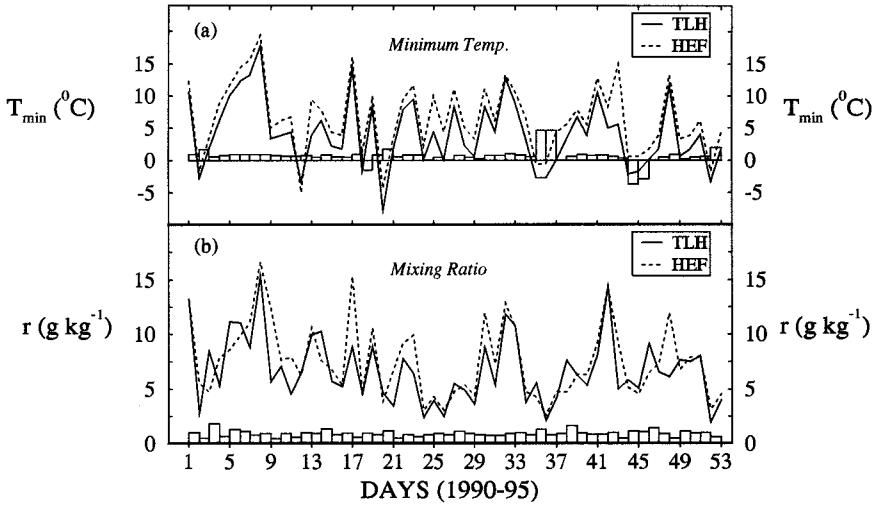

FIG. 4. (a) Observed minimum temperature (T_{min}, °C) values and (b) calculated mixing ratio values (r, g kg^{-1}) at TLH and HEF for calm, clear nights selected in 1990–95. The ratio of each observation (HEF/TLH) is shown in bars.

Unauthenticated | Downloaded 03/27/23 11:23 PM UTC

a. Model equations

Potential temperature θ, specific humidity q, and horizontal components of the wind V_h (u and v) are calculated as follows:

$$\frac{\partial V_h}{\partial t} = \frac{\partial}{\partial z}\left(K_m \frac{\partial V_h}{\partial z}\right) - w\frac{\partial V_h}{\partial z}, \tag{1}$$

$$\frac{\partial \theta}{\partial t} = \frac{\partial}{\partial z}\left[K_h\left(\frac{\partial \theta}{\partial z} - \gamma_\theta\right)\right] - w\frac{\partial \theta}{\partial z}, \tag{2}$$

$$\frac{\partial q}{\partial t} = \frac{\partial}{\partial z}\left(K_h \frac{\partial q}{\partial z}\right) - w\frac{\partial q}{\partial z}, \tag{3}$$

where K_m and K_h are the eddy diffusivities for momentum and heat, respectively, and γ_θ is the countergradient correction for potential temperature. Only the vertical diffusion terms due to boundary layer mixing and the vertical advection terms due to a prescribed vertical motion are considered in order to evaluate these equations. In the model, V_h, θ, and q are calculated at the computational levels while $\partial V_h/\partial z$, $\partial\theta/\partial z$, and $\partial q/\partial z$ are calculated between computational levels. We estimate w using the method of O'Brien (1970), which is a correction to the traditional kinematic method.

The countergradient correction term in (2) for potential temperature represents nonlocal influences on the mixing by turbulence (Deardorff 1972). Since transport of heat by turbulent eddies can be assumed to be small at night, this correction term is neglected for stable conditions. The term is evaluated in terms of surface flux of potential temperature $(\overline{w'\theta'})_s$, the boundary layer depth h, and a nondimensional constant C, which is taken as 8.5 following Holtslag (1987):

$$\gamma_\theta = \begin{cases} 0, & \text{stable,} \\ C\dfrac{(\overline{w'\theta'})_s}{w_s h}, & \text{unstable,} \end{cases} \tag{4}$$

where w_s is the velocity scale of the ABL and z_s is the top of the surface layer ($0.1h$ in the model). It depends on stability and h as shown:

$$w_s = u_*(\Phi_m)^{-1}\left(\frac{z_s}{L}\right), \tag{5}$$

where u_* and L denote the surface friction velocity and Monin–Obukhov length, respectively. The nondimensional profile functions for the shear and temperature gradients are taken from Businger et al. (1971) with modifications by Holtslag (1987).

b. Surface layer model

The surface fluxes are parameterized following Mahrt (1987) for the stable case and following Louis et al. (1982) for the unstable case as

$$u_*^2 = C_m(V_o), \tag{6}$$

$$(\overline{w'\theta'})_s = C_h(\theta_s - \theta_o), \tag{7}$$

and

$$(\overline{w'q'})_s = C_h(q_s - q_o), \tag{8}$$

where C_m and C_h are the stability-dependent surface exchange coefficients for momentum and heat, respectively. These exchange coefficients are also functions of the roughness length of heat Z_{OH} and momentum Z_{OM}. The wind speed is evaluated at the first model level (60 m for the stable case) above the surface. The surface fluxes are influenced by the interaction of the vegetated surface over land. The surface ABL parameterizations of the model allow for a distinction of direct evaporation from the soil and transpiration by the vegetation. The latent heat flux might be weak during the night as was indicated, for example, by Kondo et al. (1992). Our tests using the model also showed that the latent heat flux is negligible enough in comparison with sensible heat flux during clear, calm synoptic conditions; therefore, it does not play a very important role in the surface energy balance at night under the conditions studied here, although we acknowledge that it could be a factor in other cases. As a result, we will concentrate on sensible heat flux in our analysis. Since the latent heat flux can be neglected at nighttime, changes in the sensible heat flux will greatly affect the Bowen ratio in the model forecast.

The length scale for the surface layer is the Monin–Obukhov length as shown below:

$$L = -\frac{\theta_{\mathrm{sv}} u_*^3}{gk(\overline{w'\theta'})_s}, \tag{9}$$

where surface virtual potential temperature is denoted as θ_{sv}, g is the gravitational acceleration ($g = 9.8$ m s^{-2}), and k is the von Kármán constant (0.4 in the model). The Monin–Obukhov length is used in the nondimensional profile functions. The only variables needed to close the surface layer model are q_s and θ_s. They are available from the soil model and the surface energy balance calculation, respectively. The surface-specific humidity q_s is calculated as follows:

$$q_s = q_o + \frac{E}{\rho_o C_h}, \tag{10}$$

where q_o is the specific humidity at the air–soil interface ($z = 0$) at the first model level, E is the total evaporation, and ρ_o is the air density at the surface. Further information about the soil model can be found in Mahrt and Pan (1984) and Pan and Mahrt (1987). The soil hydrology is modeled for the nondimensional volumetric water content.

Following Troen and Mahrt (1986), the surface energy balance may be written as

Unauthenticated | Downloaded 03/27/23 11:23 PM UTC

$$\underbrace{(1-\alpha)S\downarrow}_{\text{term 1}} + \underbrace{L\downarrow}_{\text{term 2}} - \underbrace{\sigma\theta_s^4\uparrow}_{\text{term 3}} = \underbrace{G\downarrow}_{\text{term 4}} + \underbrace{H\uparrow}_{\text{term 5}} + \underbrace{L\times E\uparrow}_{\text{term 6}}, \quad (11)$$

where each term is expressed in Watts per square meter. Term 1 is downward solar radiation. The nondimensional coefficient α is the surface albedo and is a function of surface characteristics. Term 2 is downward atmospheric radiation (positive downward). Term 3 is upward terrestrial radiation; σ is the Stefan–Boltzmann constant, taken as 5.6696×10^{-8} W m^{-2} K^{-4}. Term 4 is soil heat flux (positive downward). Term 5 is sensible heat flux (positive upward). It is defined as

$$H = \rho_o C_p C_h(\theta_s - \theta_o), \quad (12)$$

and is a function of air density ρ_o, specific heat C_p that is 1004.5 J kg^{-1} K^{-1} for air, a stability-dependent exchange coefficient C_h, and the difference between the surface temperature θ_s and the air potential temperature at the first model level θ_o. Term 6 is the latent heat flux (positive upward), where L (2.5×10^6 J kg^{-1}) is the latent heat of vaporization. Total evaporation E is obtained by adding the direct soil evaporation, the transpiration, and the canopy evaporation (Mahrt and Pan 1984).

In the model, the surface energy balance is solved to derive an effective radiative (skin) surface temperature as indicated in Pan and Mahrt (1987). Incoming atmospheric longwave radiation is parameterized according to Satterlund (1979) and the incoming solar radiation is calculated following the method of Kasten and Czeplak (1980). The model predicts cloud cover using the generalized equation CLC = $f(\overline{\text{RH}}, \sigma_{\text{RH}})$, where CLC is the fractional cloud cover, $\overline{\text{RH}}$ is the maximum relative humidity in the boundary layer, and σ_{RH} is the standard deviation of relative humidity accounting for the turbulent and subgrid mesoscale variations in relative humidity.

c. ABL height

The ABL height is defined as the height at which turbulent transfers of heat, momentum, and mass are significant. Even though many formulations were suggested for the determination of the ABL height, we follow the definition of Troen and Mahrt (1986) where the transition between a stable and an unstable case is continuous as shown below:

$$h = \frac{\text{Ri}_{\text{cr}}\theta_{\text{ov}}[V(h)]^2}{g[\theta_v(h) - \theta^*_{\text{ov}}]}, \quad (13)$$

where Ri_{cr} is the critical Richardson number (0.5 in the model), θ_{ov} is the reference virtual potential temperature at the first model level above the surface, and V_h is the horizontal wind velocity at level h. This approach to diagnosing the ABL height also requires the specification of a low-level potential temperature θ^*_{ov}. This low-level potential temperature can be expressed as

$$\theta^*_{\text{ov}} = \begin{cases} \theta_{\text{ov}}, & \text{stable,} \\ \theta_{\text{ov}} + C\dfrac{(\overline{w'\theta'})_s}{w_s}, & \text{unstable.} \end{cases} \quad (14)$$

Examination of (13) indicates that ABL height can be calculated for all stability conditions when the surface fluxes and profiles of θ_v and V_h are known. Because of parameterization of θ^*_{ov}, ABL height calculations may give values that are too small under very stable conditions since the surface heat flux $(\overline{w'\theta'})$ is not always negligible at night (Ruscher 1988). A minimum value of 50 m is used even if (13) results are lower than 50 m. This means that when the solar radiation vanishes and if winds are very weak, the ABL normally collapses to the first model layer. In a previous study, h values obtained from (13) were compared with those obtained from the other model formulations (e.g, Deardorff 1972; Yu 1978; Businger and Arya 1974) and it was found that Deardorff's approach is the closest one to (13) when $h = 50$ m (Kara 1996).

The canopy evaporation of free water E_c is formulated as

$$E_c = E_p\sigma_f\left(\frac{C^*}{S'}\right)^n, \quad (15)$$

where E_p is the potential evaporation; S', the saturation water content for a canopy surface, is a constant chosen to be 2 mm; σ_f is the shading factor; and n (nondimensional) is taken to be 0.5 (Pan and Mahrt 1987). The canopy water content C^* changes as follows:

$$\frac{\partial C^*}{\partial t} = \sigma_f \times \text{Precipitation} - E_c. \quad (16)$$

When the ratio of the potential evaporation to the precipitation is large in the model, the anomolies of the soil moisture and the surface heat fluxes are very small (Kim and Stricker 1996). Otherwise, the influence of the soil on atmospheric conditions will be important for a location; however, precipitation was not a factor in the present study. Soil heat flux is calculated by solving the diffusion equation for heat, and when the soil-drying period is long enough, unrealistic temperature and moisture profiles may occur in the atmosphere (Pan and Mahrt 1987). The reason is that for moist soil thermal gradients can cause large soil heat flux, which will affect the surface energy balance equation [Eq. (11)]. Therefore, the surface temperature may be calculated with a relatively large error. However, we do not expect these kinds of unrealistic profiles in the atmosphere due to horizontal advection and clear-air radiative cooling and our integration period is not very long. The soil moisture content is also related to transpiration. The model incorporates transpiration E_t in the following manner:

Unauthenticated | Downloaded 03/27/23 11:23 PM UTC

TABLE 1. The parameters used in the initialization of the model at both sites. The symbols described in the model formulations and their units, if they exist, are in parentheses, respectively.

Parameter	TLH	HEF
Height of vegetation (d, m)	0	10
Shading factor (σ_f)	0	0.65
Plant coefficient ($k\nu$)	0	0.8
Soil moisture (%)	40	50
Soil type	Sandy clay	Clay loam
Wilting point (Θ_{wilt}, $m^3\ m^{-3}$)	0.219	0.250
Roughness length for heat (Z_{0H}, m)	0.01	0.02
Roughness length for momentum (Z_{0M}, m)	0.01	0.02

$$E_t = E_p \sigma_f k_v \frac{\sum_{i=1}^{2} [\Delta z_i g(\Theta_i)] \left[1 - \left(\frac{C^*}{S'}\right)^n\right]}{\sum_{i=1}^{2} \Delta[z_i]}, \quad (17)$$

where k_v is the plant coefficient with a value between 0 and 1. The nondimensional transpiration rate function $g(\Theta_i)$ is defined as

$$g(\Theta) = \begin{Bmatrix} 1 & \Theta > \Theta_{ref} \\ \dfrac{\Theta - \Theta_{wilt}}{\Theta_{ref} - \Theta_{wilt}} & \Theta_{ref} \geq \Theta > \Theta_{wilt} \\ 0 & \Theta_{wilt} \geq \Theta \end{Bmatrix}, \quad (18)$$

where Θ_{wilt} is the wilting point, which depends on soil characteristics such as soil type. The soil model consists of a thin upper layer (5 cm thick), which responds mainly to diurnal variation, and a thicker lower layer (95 cm thick), which participates more in seasonal changes of water storage. Therefore, i is taken as 2 in the formulation. The transpiration limits Θ_{ref} and Θ_{wilt} refer, respectively, to an upper-reference value, which is the Θ value where transpiration begins to decrease due to a deficit of water, and the plant wilting factor, which is the Θ value where transpiration stops (Mahrt and Pan 1984).

d. Model initialization

The initial vertical profiles of horizontal wind, potential temperature, and mixing ratio are determined from the appropriate operational sounding at TLH. All mandatory and significant data levels are utilized. Then data are interpolated to our vertical grid, which has layers, with 80-m vertical resolution near the surface and extends up to 200 m for the free atmosphere.

Several parameters must be input to the model to make a forecast. The two sites considered in this study have different surface properties. These are shown in Table 1. While TLH has no vegetation, HEF has a vegetation height of approximately 10 m, which is characteristic of much of the city of Tallahassee. Vegetation reduces the direct evaporation from the soil by shading the ground (Pan and Mahrt 1987). Even though the shading factor is usually 0 for TLH, HEF has a shading factor of 0.65 according to observations (H. Fuelberg 1995, personal communication).

Soil moisture and soil type are the most important parameters to be input to the model. Numerical results have shown that soil properties greatly affect ABL height and surface energy balance (e.g., Xinmei and Lyons 1995; Troen and Mahrt 1986; Mahrt and Ek 1984). These studies indicate that the impact of surface inhomogeneities in soil moisture and soil type on the atmosphere is highly dependent on the particular synoptic conditions. For this study, soil moisture measurements are not made routinely at both locations of interest since we are interested in only one type of synoptic setting. Accordingly, the volumetric soil moisture ratio (the ratio between the volumetric soil moisture content and its maximum value) is set to a value (40%) based on the Eta model results for TLH, as indicated in a previous study (Kara 1996). Determination of soil moisture at HEF is discussed in the following section.

Soil type used in the model initialization was inferred from examination of soil survey maps from the U.S. Department of Agriculture. TLH has sandy clay soil, while the soil at HEF is of clay loam type. Based on a study by Pitman et al. (1991), we can state that the hydraulic conductivity of clay is very weak. Therefore, water transport contribution in the soil may be neglected at HEF, affecting the surface energy budget with respect to soil heat flux. We will not make any attempt to discuss the effects of the physical soil properties, such as thermal diffusivity and conductivity, on the model results. In the model forecasts, the volumetric wilt point values are taken as 0.219 ($m^3\ m^{-3}$) and 0.250 ($m^3\ m^{-3}$) for sandy clay and clay loam, respectively (Clapp and Hornberger 1978). Ground heat flux is usually greater for bare-soil surfaces than for vegetated surfaces provided that there are the same net radiation conditions as Xinmei and Lyons (1995) show in their reference to Choudhury et al. (1987). This is explored in terms of surface energy balance, especially sensible heat flux, at HEF.

A proper choice of roughness length is necessary since surface layer parameterization is sensitive to these values (Beljaars and Holtslag 1991; Garratt and Pielke 1989). In many models, the roughness lengths are often taken equal to each other (i.e., $Z_{OH} = Z_{OM}$), while the roughness length for momentum (Z_{OM}) is generally at least one order larger than the one for heat (Z_{OH}) over homogeneous vegetated surfaces (Garratt 1978; Brutsaert 1982). Based on aircraft measurements and ground-based radiometric observations of surface temperature, Garratt (1978) proposed that roughness lengths for momentum and heat are between 0.4 ± 0.2 m and 0.035 ± 0.02 m, respectively, for a surface with sandy soil, 8-m-high trees, and 1-m-high dry grass. The ratio Z_{OM}/Z_{OH} was found to be approximately 12 for that kind of vegetation area. Also, Arya (1975) indicated that

Unauthenticated | Downloaded 03/27/23 11:23 PM UTC

trees have a large effect on the vertical momentum transfer so roughness elements can be expected at HEF.

In the model used here, the vegetation system is very sensitive to Z_{OM}/Z_{OH}, and the best agreement for the ABL parameters can be obtained by using a roughness length of heat that is three orders of magnitude smaller than that of momentum when one considers the analysis over heterogeneous vegetation (Holtslag and Ek 1996). An increased roughness parameter together with an increased displacement height can result in a decrease in the wind speed and thereby a decrease in the ABL height. Besides, Zhang and Anthes (1982) showed that the heat flux is reduced due to stronger evaporation as the roughness length increases. The increased evaporation and reduced depth of the ABL associated with a high roughness length increases the low-level moisture. Examination of Cabauw data (Beljaars and Holtslag 1991) showed that Z_{0M} is relatively small in the winter in comparison with summer. Under these circumstances, we used the same values of 0.01 m for both the roughness length of heat and momentum as was typically considered in atmospheric modeling studies since the TLH site is covered by very short grass indicating a plain surface. On the other hand, we increased Z_{OM} and Z_{0H} values slightly with equal values of 0.02 m due to the vegetation amount at the HEF site. These values are also consistent with the ''Davenport roughness classification'' updated by Wieringa (1992) who examined data obtained from more than 60 field experiments. Since the TLH minimum temperature anomaly is most common during the cool season, and since we determined our cases at that time, selection of Z_{OM} equal to Z_{OH} is acceptable. We will later discuss sensitivity of the model to the Z_{OM} and Z_{OH} values.

4. Minimum temperature estimates

a. The model forecasts

Temperature advections can have a considerable influence on the evolution of the nocturnal boundary layer; however, since we are interested in the TLH minimum temperature anomaly, which occurs on clear, calm nights, the one-dimensional ABL model is appropriate. In this study, the relative errors in the prediction of minimum temperature by the model are investigated using different statistical methods in terms of ABL height and the surface fluxes. In fact, one of the purposes of this study is to explore whether the model can be used as a forecast tool to predict the minimum temperature at two nearby locations that have different surface characteristics, for example, vegetation and a shading factor.

The model was initialized with upper-air sounding at 0000 UTC and a 12-h forecast was made at both locations every night. The upper-air information taken at TLH is assumed to be the same for HEF. Therefore, to represent HEF in the model analysis, only surface data (air temperature, wind speed/direction, mixing ratio, surface pressure) are changed in the sounding taken at TLH. After performing a forecast, we obtain the minimum temperature from the model called T_{mod} and compare it with the observed minimum temperature (T_{obs}). Several different statistical parameters are used to compare our model results with observations: correlation coefficient r, bias, root-mean-square error (rmse), and root-mean-square persistence (pers), given as

$$r = \frac{\sum M_{mod} M_{obs}}{N}, \tag{19}$$

$$\text{bias} = \overline{M_{mod} - M_{obs}}, \tag{20}$$

$$\text{rmse} = \sqrt{\frac{\sum (M_{mod} - M_{obs})^2}{N}}, \tag{21}$$

$$\text{pers} = \sqrt{\frac{(M_{obs-1} - M_{obs+1})^2}{N}}. \tag{22}$$

Model error statistics are computed from normalized values of T_{mod} and T_{obs} by subtracting the mean and dividing by the standard deviation, $M_i = (T_i - \overline{T_i})/\sigma_i$ where i = mod or obs.

We start the model analysis by determining the soil moisture value at HEF since we do not have any measured soil moisture data. A suitable value for the soil moisture may be determined by using the minimum temperature forecasts for several different days randomly selected in 1991–92 when there were calm, synoptic conditions over the location. At this location, because of vegetation characteristics, we used four different soil moisture values greater than 40%, which is the value at TLH, and compared the values of T_{mod} and T_{obs}. We then excluded this dataset ($n = 14$ out of the total 67 cases) from the rest of the analysis. The idea is to discard the data used in setting various model parameters. By examining the accuracy of the T_{mod} values in comparison with the T_{obs} ones, we obtain the suitable soil moisture value. Table 2 clearly indicates that using a 50% soil moisture value gives better temperature estimates from the model forecasts. Even though we have the same correlation and rmse values when 50% and 70% values were used, the mean value for T_{mod} (4.36°C) is close to

TABLE 2. The minimum temperature forecasts used for determining the soil moisture value at HEF. Correlation coefficient between the observed minimum temperatures and the model minimum temperatures is shown as $r(T_{obs}, T_{mod})$. Mean and standard deviations are also indicated; $n = 14$ for each category.

Soil moisture	T_{obs}	40% T_{mod}	50% T_{mod}	60% T_{mod}	70% T_{mod}
$r(T_{obs}, T_{mod})$		0.90	0.92	0.82	0.92
rmse (°C)		0.45	0.39	0.61	0.39
pers (°C)		1.64	1.69	1.69	1.68
Mean value (°C)	3.94	4.33	4.36	5.78	5.76
Std dev (°C)	3.65	5.86	5.86	4.57	4.96

Unauthenticated | Downloaded 03/27/23 11:23 PM UTC

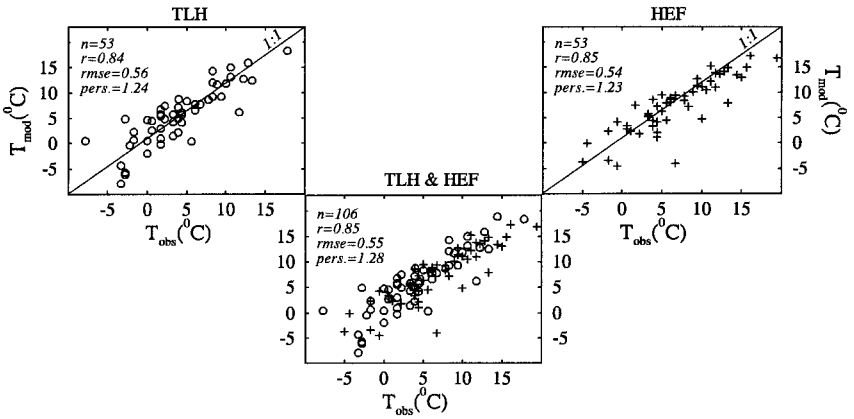

FIG. 5. Scatterplots between T_{obs} and T_{mod} values. The middle panel shows the total number of cases for both locations (TLH and HEF). The number of cases *n*, *r*, rmse (°C), and pers (°C) are also shown.

that of T_{obs} (3.94°C). As a result, the 50% value is chosen.

For all of the 53 days selected (see Fig. 4), a 12-h model forecast initialized at 0000 UTC was executed. Comparisons of the T_{obs} with the T_{mod} are shown in Fig. 5 with the scatter diagrams for TLH and HEF, separately and together. In general, the model predicts the minimum temperature reasonably well at both locations with a correlation coefficient of 0.85 and rmse of 0.55°C as one can notice little scatter. The additional statistics may be seen for each individual location from the plots in Fig. 5. The small differences between the observed and the model minimum temperatures verify that the model is able to predict well the temperatures at night, despite the fact that the horizontal advection terms in the model are missing. It is also noted that the model may be able to account for the higher minimum temperature HEF compared with TLH. We found similar bias values (0.31°C for TLH and 0.29°C for HEF) for both locations further substantiating the good agreement between model and observations.

To have a general idea of the strong cooling at TLH, turbulent fluxes and downward atmospheric radiation are examined. We use the inversion layer heat budget following André and Mahrt (1982) as

$$\underbrace{\frac{\partial \overline{T}}{\partial t}}_{\text{term 1}} = \underbrace{-\frac{\partial}{\partial z}\overline{w'T'}}_{\text{term 2}} \underbrace{-\frac{1}{\rho C_p}\frac{\partial F}{\partial z}}_{\text{term 3}} + \underbrace{A}_{\text{term 4}}, \quad (23)$$

TABLE 3. Averaged heat budget over the depth of turbulent layer h_R and inversion layer h_s at night for TLH. Percentage values are in parentheses and all are in (10^{-2} K m s^{-1}); $n = 53$ for each layer.

	$C = \int_0^h \frac{\partial T}{\partial t}\, dz$	Q_0	ΔF	I
Turbulence layer	−7.41	−0.66 (9.0%)	−2.96 (39.9%)	−3.79 (51.1%)
Inversion layer	−1.87	−0.66 (35.4%)	−2.07 (110.6%)	0.86 (−46.0%)

where the temperature change (term 1) consists of turbulent flux (term 2), the net longwave radiative flux (term 3), and the residual *A* (term 4) due to errors in the estimation of other terms.

Integrating (23) from the surface to the depth of the turbulence layer and to that of the inversion layer yields the results shown in Table 3 at TLH. The 12-h vertically integrated forms of all terms show in (23) are symbolized as *C*, Q_0, ΔF, and *I*, respectively. The depth of turbulent layer h_R was determined using the ABL height profiles obtained from the model, while the depth of the inversion layer h_s was obtained from the potential temperature and wind profiles for each night. The temperature change *C* was computed from the 12-h upper-air soundings. The turbulent heat fluxes and radiative fluxes obtained from the model were averaged for each individual case, then the results obtained were averaged over all 53 cases. Table 3 clearly explains that clear-air radiative cooling dominates turbulent cooling in both turbulence layer and inversion layer. Even in the turbulence layer, cooling due to clear-air effects (39.9%) is almost five times greater than turbulence cooling (9.0%). This means that clear-air radiative cooling dominates the heat budget for both the inversion layer and the turbulence layer on clear, calm synoptic conditions over TLH. We also notice a very large residual *I* in the turbulence layer. This large error in the residual (51.1 %) can be attributed to estimates of the surface heat fluxes, which involve stability-dependent coefficients C_m and C_h used in (6)–(8).

b. Sensitivity to roughness lengths

We used different values for roughness length of heat and momentum by keeping the other parameters constant (see Table 1) in the model initialization and performed forecasts to examine the effects of roughness length on the minimum temperature estimates. We mainly concentrated on Z_{OM} values by changing them to sev-

Unauthenticated | Downloaded 03/27/23 11:23 PM UTC

TABLE 4. Comparisons between T_{obs} and T_{mod} values in terms of r, rmse, and pers for different sets of Z_{OH}, when Z_{OM} is taken as 0.01 m. Values in parentheses show results when Z_{OH} is taken as 0.1 m. The percentage increase in r for each case is shown as $r \uparrow (T_{obs}, T_{mod})$ (%). All values are for TLH; $n = 53$ for each category.

Z_{OM}	0.1	0.5	1	2	3
B^{-1}	5.8	9.8	11.5	13.2	14.3
	(0)	(4.0)	(5.8)	(7.5)	(8.5)
r (T_{obs}, T_{mod})	0.76	0.77	0.77	0.77	0.78
	(0.78)	(0.80)	(0.81)	(0.81)	(0.80)
$r \uparrow$ (T_{obs}, T_{mod}) (%)	2.6	3.9	5.2	5.2	2.6
rmse (°C)	0.69	0.67	0.67	0.68	0.66
	(0.66)	(0.62)	(0.61)	(0.61)	(0.63)
pers (°C)	1.31	1.27	1.27	1.28	1.27
	(1.34)	(1.32)	(1.32)	(1.31)	(1.30)

eral orders of magnitude greater than Z_{OH} since momentum transport is influenced by forces at obstacles, while heat is not influenced by these kinds of forces over homogeneous terrain. On the other hand, we selected Z_{OH} as 0.1 m and 0.01 m to test all the different Z_{OM} values. According to the definition of Brutseart (1982), we also calculated $B^{-1} = (1/k) \ln(Z_{OM}/Z_{OH})$ values.

Different sets showing the sensitivity of the model behavior to Z_{OH} and Z_{OM} can be seen from Tables 4 and 5. When $B^{-1} = 0$ (in other words, $Z_{OH} = Z_{OM}$), the minimum temperature forecasts give good results. It appears that the minimum temperature forecast is more sensitive to selection of roughness lengths at HEF than at TLH due to vegetation characteristics. For example, when $Z_{OH} = 0.01$ m for all Z_{OM} values at HEF, r varies between 0.73 and 0.78. However, r is almost constant with values of 0.77 or 0.78 for the same category at TLH. Taking $Z_{OM} = 2$ m for $Z_{OH} = 0.01$ m and for $Z_{OH} = 0.1$ m at TLH yields r values 0.77 and 0.81, respectively, whereas r increases from 0.73 to 0.80 (9.6%) at HEF, which corresponds to typically larger rmse's than those at TLH. This also indicates that changes in Z_{OH}, even one order of magnitude (from 0.01 m to 0.1 m), affect the forecasts at HEF, especially for $Z_{OM} \geq 1$. Also notice that there is no change in the forecasts at HEF when B^{-1} has values of 5.8 and 0, respectively. The same is true for B^{-1} values of 9.8 and 4.0. On the other hand, r corresponding to these B^{-1} values increases slightly at TLH, which explains why Z_{OM} should be of the same order as Z_{OH}. As a result, when B^{-1} decreases for any value of Z_{OM}, the results tend to be improved for all cases at both locations. This shows that taking Z_{OM} at least two orders of magnitude greater than Z_{OH} results in a poor forecast. However, Z_{OM} at the same order or one order greater than Z_{OH} yields good forecasts. In general, examination of r, rmse, and pers for the total 1060 model forecasts shown in Tables 4 and 5 confirms that using different sets for Z_{OM} and Z_{OH} may result in serious errors in comparison with our selection shown in Table 1, especially for HEF.

TABLE 5. As in Table 4 but for HEF.

Z_{OM}	0.1	0.5	1	2	3
B^{-1}	5.8	9.8	11.5	13.2	14.3
	(0)	(4.0)	(5.8)	(7.5)	(8.5)
r (T_{obs}, T_{mod})	0.78	0.76	0.76	0.73	0.74
	(0.78)	(0.77)	(0.79)	(0.80)	(0.79)
$r \uparrow$ (T_{obs}, T_{mod}) (%)	0.0	1.3	4.0	9.6	6.8
rmse (°C)	0.67	0.69	0.69	0.74	0.73
	(0.66)	(0.70)	(0.65)	(0.64)	(0.65)
pers (°C)	1.28	1.26	1.32	1.30	1.28
	(1.32)	(1.30)	(1.29)	(1.29)	(1.30)

5. Results and discussion

To further examine the model performance on predicting the minimum temperature, we also investigate the observed and model minimum temperature relations in terms of ABL height obtained from the 12-h forecasts. First, we evaluated the general behavior of ABL height for a 12-h period. We will later discuss the effects of ABL height on minimum temperature estimates at the time when the minimum temperature is predicted instead of examining the 12-h changes. We obtained ABL height from the model for each individual day (total 53 days for each location) at night and determined how the ABL height changed during the 12-h period starting at 0000 UTC. We separated the cases into three categories: 1) collapse of the ABL (c), 2) growth of the ABL (g), and 3) neither growth nor collapse (n).

Figure 6 is the comparison between T_{obs} and T_{mod} for the three cases. As an example of how we determined the collapse of the ABL, an individual case is shown inside the first panel at TLH, indicating the changes of ABL height with time on 9 February 1993. We found this kind of ABL height profile 30 days out of 53 days at TLH. Examples of the cases when there was growth or when there was neither growth nor decay in the ABL can also be noticed from Fig. 6 on 7 December 1994 and on 26 November 1995, respectively. The number of cases ($n = 14$ days) when the ABL grew at HEF is greater than that at TLH. This is due to the increasing sensible heat flux, which has an average value of 8.4 W m^{-2} that is calculated at HEF considering all cases. We found a relatively small average sensible heat flux value (5.5 W m^{-2}) at TLH. Figure 6 also illustrates that there is not a strong relationship between the model and observed minimum temperatures when the ABL height neither grew nor decayed. In these cases, correlation coefficients are 0.72 and 0.78 for TLH and HEF, respectively, which are significantly smaller than the other categories. The ratio of mean T_{obs} values (8.4°C) to T_{mod} values (7.3°C) is also largest at HEF among the other categories when the ABL neither grew nor collapsed. This explains that the model predicts the minimum temperatures best when there is, in general, a growth or collapse of the ABL during the 12-h period at night. The significance of the correlation coefficients calculated for each case was also tested with a student-t dis-

Unauthenticated | Downloaded 03/27/23 11:23 PM UTC

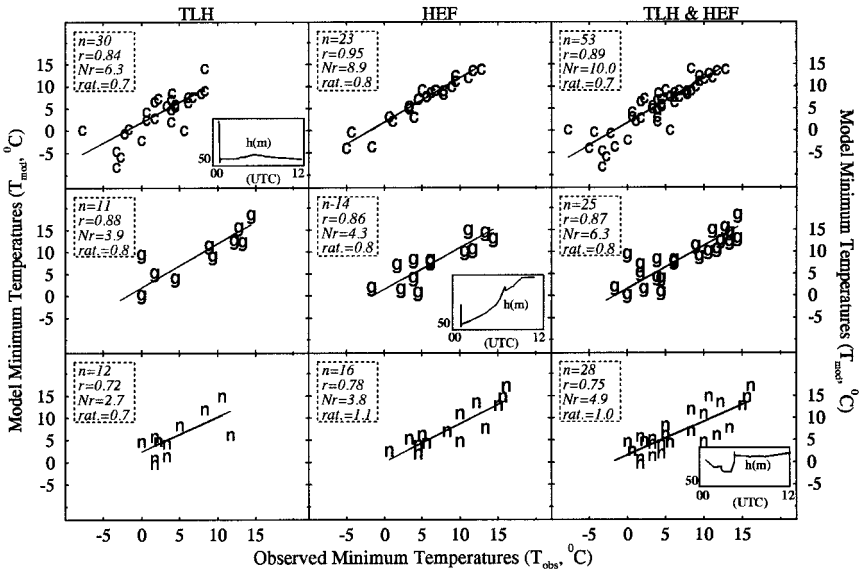

FIG. 6. Comparisons between T_{obs} and T_{mod} when the ABL completely collapsed (shown as *c*), when it grew (shown as *g*), and when it neither grew nor collapsed (shown as *n*) for each day selected in 1990–95 for a 12-h period at night. Examples of collapsing, growing, and neither of them in the ABL *h* are plotted in the panels. The number of cases *n*, correlation coefficient *r*, significance of correlation coefficient Nr, and ratio of T_{obs} to T_{mod} (rat. = T_{obs}/T_{mod}) is also shown for each category.

tribution by using the null hypothesis at the $\alpha = 0.05$ level (Bendat and Piersol 1986). The corresponding values (Nr) are written in Fig. 6 and indicate that observed temperatures are well correlated to the model ones for each category since none of the Nr values fall inside the region ± 1.96. Combining the cases from TLH and HEF, we notice that the best agreement is found for the forecasts when the ABL height collapsed at night, with a correlation of 0.89, and with a mean ratio (T_{obs}/T_{mod}) of 0.7.

To examine the source of cooling, we plotted the scaled curvature of the potential temperature γ against the bulk (Richardson number (Fig. 7a) obtained from the model at 0100 and 0700 LST. The γ values [André and Mahrt (1982)] are calculated using the potential temperature and surface-inversion height h_s profiles as shown below:

$$\gamma = \frac{\theta(h_s) - 2\theta(h_{s/2}) + \theta(0)}{\theta(h_s) - \theta(0)}, \tag{24}$$

where 0 represents the surface level. As seen from the large scatter in Fig. 7a, the relationship between γ and Ri_B is very weak at both 0100 and 0700 LST. We still notice several large negative γ values at 0100 LST, due possibly to remnants from convective mixing in the previous daytime ABL. As a result of the incoming solar radiation leading to strong heating of the ground during early morning, we find some cases where the Ri_B is less than 1. In the morning at 0700 LST, we notice the existence of large negative γ values corresponding to large Ri_B values around -10. However, the number of cases at 0100 LST is greater than at 0700 LST when Ri_B is large positive and some of these cases correspond again to large negative γ values. From Fig. 7a, we also notice

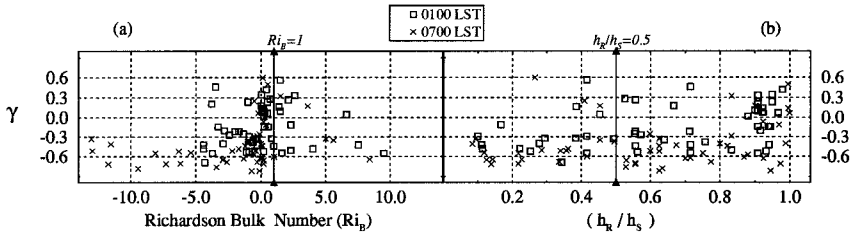

FIG. 7. (a) Scaled curvature of the potential temperature profile γ vs the bulk Richardson number (Ri_B) obtained from the model at TLH for 0100 and 0700 LST. (b) Scaled curvature γ vs ratio of the turbulent nocturnal ABL to surface inversion (h_R/h_s) for the same time intervals shown in (a) at TLH.

Unauthenticated | Downloaded 03/27/23 11:23 PM UTC

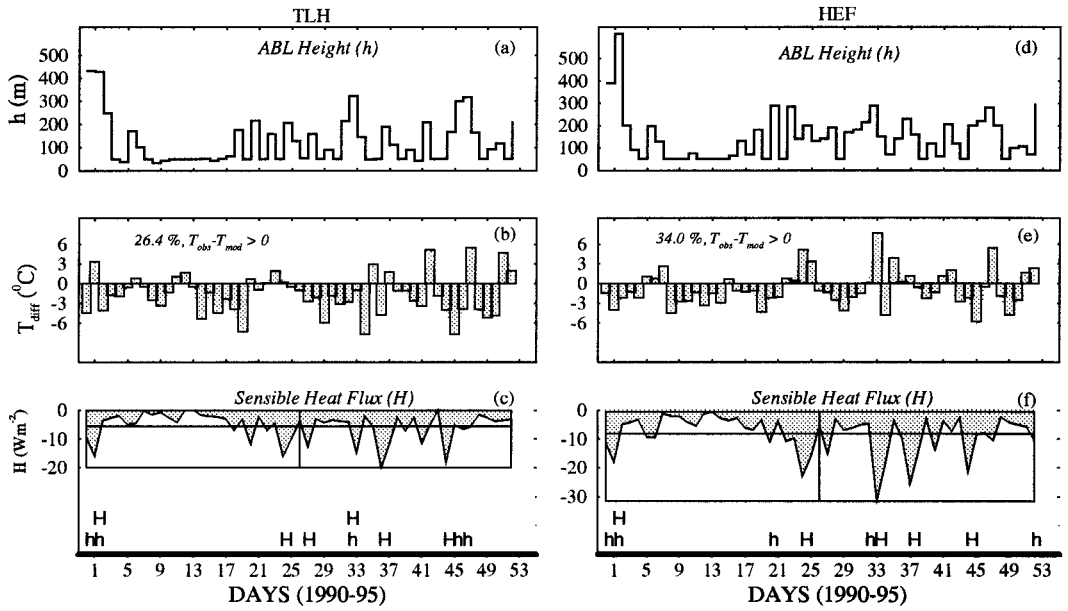

FIG. 8. (a) ABL height (h) when the minimum temperature was predicted by the model, (b) the minimum temperature difference T_{diff} between T_{obs} and T_{mod}, and (c) 12 h-averaged value of the sensible heat flux (H) at night for each day at TLH. Panels (d), (e), and (f) are the same as (a), (b), and (c), respectively, but for HEF. Horizontal lines in (c) and (f) show the average of all 12-h-averaged values (see text). In the bottom diagrams *H* indicates cases when peaks in sensible heat flux occurred, and *h* when significant peaks of ABL *h* occurred.

that the relationship between γ and Ri_B tends to be down for positive Ri_B numbers due to increasing stability and decreasing turbulence activity at 0100 LST. Later in the morning as soon as the wind picks up, possibly enhanced by jet plane activity, the gradient gets large, which reduces the Richardson number values to near 1, eroding the inversion with turbulence. At this time, turbulence is a heating process since it tries to make the atmosphere adiabatic. In summary, scaled curvature of the potential temperature increases; in other words, it tends to be positive when the turbulence becomes strong enough to cover most of the inversion layer (see also Fig. 7b).

Since γ depends on h_s, we examined the ratio of the depths of turbulent nocturnal ABL and surface inversion h_R/h_s with respect to γ (Fig. 7b) at TLH. When h_R becomes very close to h_s (for example, $0.8 < h_R/h_s < 1.0$), we have more cases at 0100 than at 0700 LST. When $h_R/h_s > 0.5$, there are 38 cases at 0100 LST, while there are 32 cases when $h_R/h_s > 0.5$ at 0700 LST, showing that the depth of surface inversion increases especially after midnight since the depth of the turbulence layer usually changes slowly with time at night. We also notice that there are only a few cases when h_s is much greater than h_R (see $0 < h_R/h_s < 0.2$ in Fig. 7b). Therefore, a relatively small thickness of the turbulence layer compared with the depth of the inversion layer explains that the inversion layer is dominated by clear-air radiative cooling. Besides, the increase in thickness of the inversion layer is more related to clear-air radiative cooling. Also note that γ has typically large negative values at both 0100 and 0700 LST indicating the existence of the large surface heat fluxes. On these days, the ABL height is relatively small as expected (see also Figs. 8a,c). Large γ values also indicate strong stratification in the lower part of the inversion layer at TLH since stratification is usually small at the top of the inversion layer (André and Mahrt 1982). We also noticed that the average of γ values (-0.14) at 0100 LST is smaller than that of γ values (-0.41) at 0700 LST in the morning, which indicates the dominant effect of clear-air radiative cooling.

We also examined if a significant change in ABL height and in surface fluxes, in particular sensible heat flux *H*, leads to any changes in minimum temperature forecasts (see Fig. 8). We obtained ABL height from the model at the time of the minimum temperature prediction for each individual day, while *H* was averaged over the 12-h period to represent the whole night. There were five cases for both TLH and HEF when significant peaks of ABL height occurred (Figs. 8c,f). Minimum temperature differences when significant peaks of ABL height occurred were $[-2.8°\text{C} > (T_{\text{obs}} - T_{\text{mod}}) > -6.7°\text{C}]$ for TLH and $[-1.4°\text{C} > (T_{\text{obs}} - T_{\text{mod}}) > -4.0°\text{C}]$ for HEF except for two cases when positive temperature differences (3.3°C at TLH and 2.3°C at HEF) were found. These temperature differences are the largest ones overall (Figs. 8b, e); therefore, it is suggested that the prediction of minimum temperature by the model is less accurate when ABL *h* is large. We also notice that $(T_{\text{obs}} - T_{\text{mod}})$ values are usually negative at both locations. This is possibly due to the fact that all our cases are chosen from the cool season and warm-air advection

Unauthenticated | Downloaded 03/27/23 11:23 PM UTC

might have some influence on the forecasts (Sorbjan 1995).

There were six cases for TLH and five cases for HEF when significant peaks of H were observed. When significant peaks of H occurred ($T_{obs} - T_{mod}$), values are still large. There are only two cases (27 January 1990 and 7 December 1994) when the peaks in both ABL height and sensible heat flux occurred at TLH, while at HEF there is only one case (27 January 1990), as can be seen from Figs. 8c,e, respectively. On these days, observed minimum temperatures were approximately 3°C warmer than the model minimum temperatures.

Finally, we proceed with the results for the atmospheric variables, in particular the air temperature, potential temperature, relative humidity, and horizontal wind speed, to illustrate the model performance for TLH at 0000 UTC. We calculated these atmospheric variables at each 20-m interval for all individual days using the model results and averaged over the number of cases (53 days) at each 20-m height interval. When required for any of the calculations, linear interpolation between levels was used. To calculate the observed profiles at 0000 UTC, upper-air soundings at TLH were used and the above similar procedure at each 20 m was applied. The profiles up to 1500 m are shown in Fig. 9, indicating that all simulations are quite good, with deviations between observed and computed variables being very small most of the time. Also, the model results agree best with the observed values, in particular for air temperature and relative humidity. The model results for temperatures are colder and more humid in comparison with the observations. The error in the prediction of wind speed is relatively large—a 1.2 m s^{-1} value between 250 and 750 m. The model profiles can be improved by including the influence of advection.

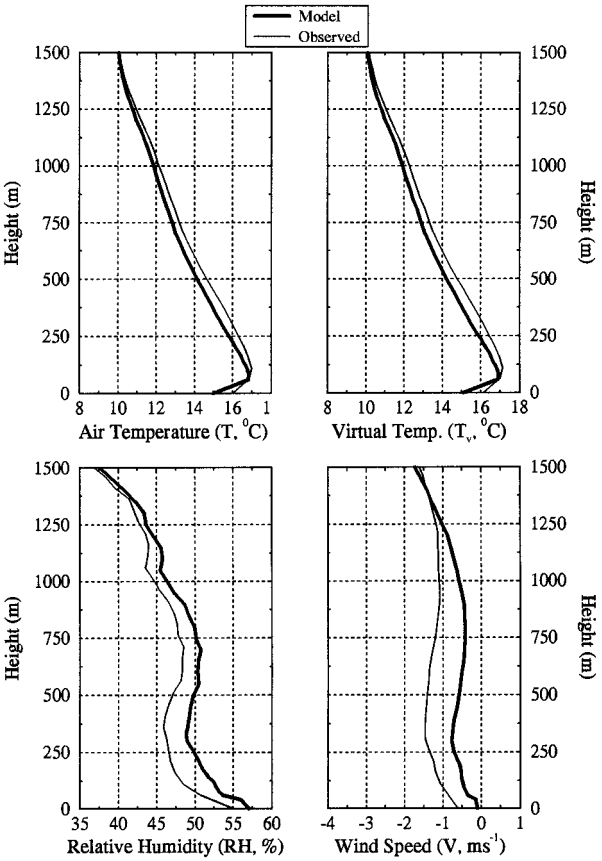

FIG. 9. Averaged profiles over TLH at 0000 UTC for air temperature (°C), virtual temperature (°C), relative humidity (%), and wind speed (m s^{-1}) from the upper-air soundings (thin lines) and from the corresponding averaged model profiles for all 53 cases selected in 1990–95.

6. Conclusions

The TLH nocturnal minimum temperature anomaly (Elsner et al. 1996) is examined in detail with the aid of the one-dimensional Oregon State University atmospheric boundary layer (ABL) model, coupled to the soil model. The model is used to make 12-h forecasts of ABL parameters at TLH and an adjacent site (HEF) located 16 km northeast of TLH. Under clear, calm synoptic situations during the cool season, TLH nighttime minimum temperatures are often several degrees lower than the HEF site. Even though these two sites have different surface characteristics, the model is able to forecast the nocturnal evolution of the boundary layer at both sites with reasonable accuracy, including the surface air temperatures. In particular, the model results are the best when the ABL collapses at night.

Both soil moisture and roughness length have a large effect on the minimum temperature forecasts. Our discussions show that it is necessary to use proper values for both roughness length of heat and momentum. Selection of these parameters is important, especially for a location covered by high vegetation. Forecast comparisons indicate that the lower minimum temperatures at TLH are related to clear-air radiative cooling throughout the inversion layer. In particular, negative values of the scaled curvature of potential temperature when examined with respect to bulk Richardson number indicate strong stratification in the lower part of the inversion layer owing to the dominant effect of clear-air radiative cooling at TLH. This study can be improved by examining the temperature advection, so that the errors between observed temperatures and model temperatures can be determined. Temperature changes due to longwave radiation can be compared to the ones due to advection. Since the model is sensitive to the initial value of the roughness length, a 10- or 15-min wind speed/direction observation can be used to determine this parameter. We determined the soil moisture based on Eta model results. It is possibly a source of error. In addition, the model sometimes tends to produce clouds too efficiently because of unrealistically large moisture mixing; therefore, work is in progress to examine more accurate representations of boundary layer clouds.

Unauthenticated | Downloaded 03/27/23 11:23 PM UTC

Acknowledgments. We are grateful to Professor H. E. Fuelberg for his personal data archive and his graciousness in allowing us to extract relevant information. We gratefully acknowledge the interesting comments made by reviewers. The manuscript was improved by these helpful suggestions. The support of NCAR for use of their data archive is also acknowledged. Partial support for this project came from NOAA through the Cooperative Institute on Tropical Meteorology. The views expressed herein are those of the authors and do not necessarily reflect the views of NOAA, its subagencies, or UCAR.

REFERENCES

André, J. C., and L. Mahrt, 1982: The nocturnal surface inversion and influence of clear-air radiative cooling. *J. Atmos. Sci.,* **39,** 864–878.

Anfossi, D., P. Bacci, and A. Longhetto, 1976: Forecasting of vertical temperature profiles in the atmosphere during nocturnal radiation inversions from air temperature trend at screen height. *Quart. J. Roy. Meteor. Soc.,* **102,** 173–180.

Arya, S. P. S., 1975: Geostrophic drag and heat transfer relations for the atmospheric boundary layer. *Quart. J. Roy. Meteor. Soc.,* **101,** 147–161.

Beljaars, A. C. M., and A. A. M. Holtslag, 1991: Flux parameterization over land surfaces for atmospheric models. *J. Appl. Meteor.,* **30,** 327–341.

Bendat, J. S., and A. G. Piersol, 1986: *Random Data.* Wiley Press, 566 pp.

Brutsaert, W., 1982: *Evaporation into the Atmosphere.* D. Reidel Publishing, 299 pp.

Businger, J. A., and S. P. S. Arya, 1974: Heights of the mixed layer in the stably stratified planetary boundary layer. *Advances in Geophysics,* Vol. 18A, Academic Press, 73–92.

——, J. C. Wyngaard, Y. Izumi, and E. F. Bradley, 1971: Flux-profile relationships in the atmospheric surface layer. *J. Atmos. Sci.,* **28,** 181–189.

Carlson, M. A., and R. B. Stull, 1986: Subsidence in the nocturnal boundary layer. *J. Climate Appl. Meteor.,* **25,** 1088–1099.

Choudhury, B. J., S. B. Idso, and R. J. Reginato, 1987: Analysis of an empirical model for soil heat flux under a growing wheat crop for estimating evaporation by an infrared-temperature based energy balance equation. *Agric. For. Meteor.,* **39,** 283–297.

Clapp, R. B., and G. M. Hornberger, 1978: Empirical equations for some soil hydraulic properties. *Water Resour. Res.,* **14,** 601–604.

Deardorff, J. W., 1972: Parameterization of the planetary boundary layer for use in general circulation models. *Mon. Wea. Rev.,* **100,** 93–106.

Elsner, J. B., H. E. Fuelberg, R. L. Deal III, J. A. Orrock, G. S. Lehmiller, and P. H. Ruscher, 1996: Tallahassee, Florida, minimum temperature anomaly: Description and speculations. *Bull. Amer. Meteor. Soc.,* **77,** 721–728.

Garratt, J. R., 1978: Transfer characteristics for a heterogeneous surface of large aerodynamic roughness. *Quart. J. Roy. Meteor. Soc.,* **104,** 491–502.

——, and R. A. Brost, 1981: Radiative cooling effects within and above the nocturnal boundary layer. *J. Atmos. Sci.,* **38,** 2730–2746.

——, and R. A. Pielke, 1989: On the sensitivity of mesoscale models to surface-layer parameterization constants. *Bound.-Layer Meteor.,* **48,** 377–387.

Holtslag, A. A. M., 1987: Surface fluxes, and boundary-layer scaling: Model and applications. KNMI Scientific Rep. 87-02, 14 pp. [Available from KNMI, P.O. Box 201, 3730 AE De Bilt, the Netherlands.]

——, and M. Ek, 1996: Simulation of surface fluxes and boundary layer development over the pine forest in HAPEX-MOBILHY. *J. Appl. Meteor.,* **35,** 202–213.

Kara, A. B., 1996: Analysis of boundary layer structure over and around the Gulf of Mexico. M.S. thesis, Department of Meteorology, The Florida State University, 78 pp. [Available from Dept. of Meteorology, The Florida State University, Tallahassee, FL 32306-4520.]

Kasten, F., and G. Czeplak, 1980: Solar and terrestrial radiation dependent on the amount and type of cloud. *Sol. Energy,* **24,** 177–189

Kim, C. P., and J. N. M. Stricker, 1996: Consistency of modeling the water budget over long time series: Comparison of simple parameterizations and a physically based model. *J. Appl. Meteor.,* **35,** 749–760.

Klöppel, M., G. Stilke, and C. Wamser, 1978: Experimental investigations into variations and comparisons with results of simple boundary layer methods. *Bound.-Layer Meteor.,* **15,** 135–146.

Kondo, J., N. Saigusa, and T. Sato, 1992: A model and experimental study of evaporation from bare soil surfaces. *J. Appl. Meteor.,* **31,** 304–312.

Louis, J.-F., M. Tiedtke, and J. F. Geleyn, 1982: A short history of the operational PBL Parameterization of ECMWF. *Workshop on planetary boundary Layer Parameterization,* Shinfield Park, Reading, United Kingdom, European Centre for Medium-Range Weather Forecasts, 59–79.

Mahrt, L., 1987: Grid-averaged surface fluxes. *Mon. Wea. Rev.,* **115,** 1550–1560.

——, and M. Ek, 1984: The influence of atmospheric stability on potential evaporation. *J. Climate Appl. Meteor.,* **23,** 222–234.

——, and H.-L. Pan, 1984: A two-layer model of soil hydrology. *Bound.-Layer Meteor.,* **29,** 1–20.

Nieuwstadt, F. T. M., 1980: Notes on ''A rate equation for the inversion height in a nocturnal boundary layer.'' *J. Appl. Meteor.,* **19,** 1445–1447.

——, and A. G. M. Driedonks, 1979: The nocturnal boundary layer: A case study compared with model calculations. *J. Appl. Meteor.,* **18,** 1397–1405.

O'Brien, J. J., 1970: A note on the vertical structure of the eddy exchange coefficient in the planetary boundary layer. *J. Atmos. Sci.,* **27,** 1213–1215.

Pan, H.-L., and L. Mahrt, 1987: Interaction between soil hydrology and boundary layer development. *Bound.-Layer Meteor.,* **38,** 185–202.

Pitman, A. J., Z.-L. Yang, J. G. Cogley, and A. Henderson-Sellers, 1991: Description of bare essentials of surface transfer for the Bureau of Meteorology Research Centre AGCM. BMRC Research Rep. 32, 132 pp. [Available from BMRC 3, Avenue Circulaire, Bruxelles B-1180, Belgium.]

Quinet, A., and J. Vanderborght, 1996: Clear-sky nocturnal temperatures forecast and the greenhouse effect. *J. Appl. Meteor.,* **35,** 401–415.

Ruscher, P. H., 1988: Parameterization of the very stable boundary layer in a simple model. Preprints, *Eighth Symp. on Turbulence and Diffusion,* San Diego, CA, Amer. Meteor. Soc., 299–301.

Satterlund, D. R., 1979: Improved equation for estimating long-wave radition from the atmosphere. *Water Resour. Res.,* **15** 1649–1650.

Sorbjan, Z., 1995: Toward evaluation of heat fluxes in the convective boundary layer. *J Appl. Meteor.,* **34,** 1092–1098.

Stull, R. B., 1983: *An Introduction to Boundary Layer Meteorology.* Kluwer Academic, 666 pp.

Troen, I., and L. Mahrt, 1986: A simple model of the atmospheric boundary layer model: Sensitivity to surface evaporation. *Bound.-Layer Meteor.,* **37,** 129–148.

Wieringa, J., 1992: Updating the Davenport roughness classification. *J. Wind Eng. Industr. Aerodyn.,* **41,** 357–368.

Xinmei, H., and T. J. Lyons, 1995: The simulation of surface heat fluxes in a land surface–atmosphere model. *J. Appl. Meteor.,* **34,** 1099–1111.

Yamada, T., 1979: Prediction of nocturnal surface inversion height. *J. Appl. Meteor.,* **18,** 526–531.

Yu, T.-W., 1978: Determining the height of the nocturnal boundary layer. *J. Appl. Meteor.,* **17,** 28–33.

Zhang, D., and R. A. Anthes, 1982: A high-resolution model of the planetary boundary layer—Sensivity tests and comparisons with SESAME-79 data. *J. Appl. Meteor.,* **21,** 1594–1609.

Unauthenticated | Downloaded 03/27/23 11:23 PM UTC